



# Rational Design and Synthesis of Phenethyl-5-bromopyridyl Thiourea Derivatives as Potent Non-nucleoside Inhibitors of HIV Reverse Transcriptase

Rakesh Vig,<sup>a,b</sup> Chen Mao,<sup>a,c</sup> T. K. Venkatachalam,<sup>a,b</sup> Lisa Tuel-Ahlgren,<sup>d</sup>  
Elise A. Sudbeck<sup>a,c</sup> and Fatih M. Uckun<sup>a, d,\*</sup>

<sup>a</sup>Drug Discovery Program, Hughes Institute, St. Paul, MN 55113, USA

<sup>b</sup>Department of Chemistry, Hughes Institute, St. Paul, MN 55113, USA

<sup>c</sup>Department of Structural Biology, Hughes Institute, St. Paul, MN 55113, USA

<sup>d</sup>Department of Virology, Hughes Institute, St. Paul, MN 55113, USA

Received 9 March 1998; accepted 11 May 1998

**Abstract**—A series of novel phenethylthiazolylthiourea (PETT) derivatives targeting the nonnucleoside inhibitor (NNI) binding site of HIV reverse transcriptase (RT) have been designed based on the structure of the NNI binding pocket. The structure-based design and synthesis of these new PETT derivatives were complemented by biological assays of their anti-HIV activity. Modeling studies for rational drug design included the construction of a composite NNI binding pocket from nine RT-NNI crystal structures, the analyses of surface complementarity between NNI and RT, and application of  $K_i$  calculations combined with a docking procedure involving the novel PETT derivatives. The use of the composite NNI binding pocket allowed the identification and structure-based design of three promising PETT derivatives with *ortho*-F (**2**), *ortho*-Cl (**3**), and *meta*-F (**5**) substituents on the phenyl ring. These novel PETT derivatives were more active than AZT or zidovudine and showed potent anti-HIV activity with  $IC_{50}[p24]$  values of  $< 1$  nM and selectivity indices of  $> 100,000$ . © 1998 Elsevier Science Ltd. All rights reserved.

## Introduction

Design of potent inhibitors of HIV reverse transcriptase (RT) has been a focal point in translational AIDS research efforts.<sup>1–3</sup> Among the promising inhibitors are the nonnucleoside inhibitors (NNIs), which include tetrahydroimidazobenzodiazepinethione (TIBO) compounds,<sup>4</sup> 1-[(2-hydroxyethoxy)methyl]-6-(phenylthio)-thymine (HEPT) derivatives,<sup>5–8</sup> bis(heteroaryl)piperazine (BHAP) analogues,<sup>9</sup> 2'-5'-bis-*O*-(tertbutyldimethylsilyl)-3'-spiro-5''-(4''-amino-1'', 2''-oxathiole-2'', 2''-dioxide) pyrimidine (TSAO),<sup>10</sup> and phenethylthiazolylthiourea (PETT) derivatives.<sup>11–14</sup> NNIs have been found to bind to a specific allosteric site of HIV-1 RT<sup>15–20</sup> near the polymerase site and interfere with reverse transcription

by altering either the conformation or mobility of RT, thereby leading to a noncompetitive inhibition of the enzyme.<sup>15–20</sup> A number of crystal structures of RT complexed with NNIs (including  $\alpha$ -APA, TIBO, Nevirapine, and HEPT derivatives) have been reported, and such structural information provides the basis for further derivatization of NNI aimed at maximizing binding affinity to RT.

Structure-based drug design efforts often encounter difficulties in obtaining the crystal structure of the target and predicting the binding modes for new compounds. The difficulties in translating the structural information gained from X-ray crystallography into a useful guide for drug synthesis calls for continued efforts in the development of computational tools. While qualitative assessments of RT-inhibitor complexes provide helpful information (see Hopkins et al.),<sup>21</sup> systematic quantitative prediction of inhibitory activity of new compounds based on structural information remains a challenge.<sup>22</sup>

Key words: Anti-HIV; NNI; inhibitor; modeling; drug-design.

\*Corresponding author at: Drug Discovery Program, Wayne Hughes Institute, 2665 Long Lake Road, Suite 330, St. Paul, MN 55113, USA. Tel: (651) 697-9228; fax: (651) 697-1042.

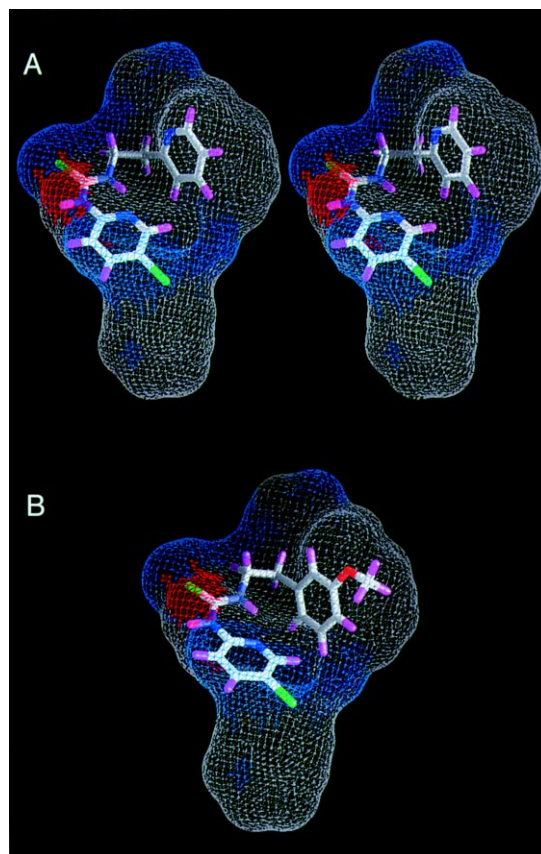
In the present study, a series of PETT derivatives have been designed based on the structure of the NNI binding pocket. The structure-based design and synthesis of these new PETT derivatives were complemented by biological assays of their anti-HIV activity. Modeling studies for rational drug design included the construction of a composite NNI binding pocket from nine RT-NNI crystal structures, the analyses of surface complementarity between NNIs and RT, and application of  $K_i$  calculations combined with a docking procedure involving the novel PETT derivatives. Our computational approach allowed the identification of several ligand derivatization sites for the generation of more potent PETT derivatives. Three promising PETT derivatives identified and characterized herein were non-cytotoxic and elicited potent anti-HIV activity with  $IC_{50}$  values less than 1 nM for inhibition of HIV replication (measured by p24 production in HIV-infected human peripheral blood mononuclear cells).

## Results and Discussion

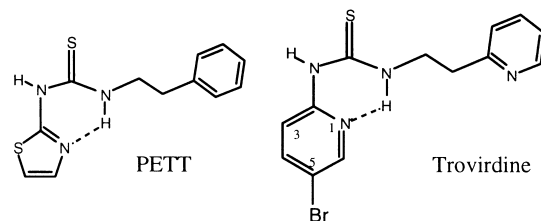
### NNI design

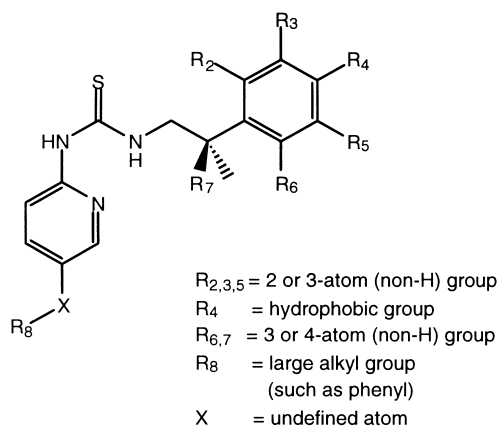
In the course of our search for potent NNIs, we developed a computer model in which a composite binding pocket was constructed from nine individual crystal structures of RT-NNI complexes (Fig. 1).<sup>23</sup> Our detailed analysis of zalcitabine, a potent PETT derivative, revealed multiple sites which can be used for the incorporation of larger functional groups. In our composite binding pocket (Fig. 1), the docked zalcitabine molecule showed abundant sterically allowed usable space surrounding the pyridyl ring, the ethyl linker and near the 5-bromo position (shown in zalcitabine structure). We hypothesized that an efficient use of this space by strategically designed functional groups should yield more potent anti-HIV agents with higher affinity for the NNI binding pocket of HIV RT. Replacement of the pyridyl ring by a piperidinyl ring or a 2,5-dimethoxyphenyl group resulted in superior inhibitory activities and strongly supported our hypothesis.<sup>23</sup> Encouraged by the successful application of our working model, we decided to investigate the effect of systematic substitutions on various positions of the phenyl ring, such as a methoxy group, fluorine atom, or chlorine atom. Through a mapping of the protein–inhibitor interactions in the region, our goal was to better understand the inhibitor binding and develop more potent inhibitors.

A computer simulation of the binding of the target PETT derivatives into the NNI binding site of RT was accomplished using a molecular docking procedure. Docking of the compounds into the NNI binding site required the use of X-ray coordinates of an RT/NNI



**Figure 1.** (A) Stereoview of zalcitabine and (B) monoview of compound **4** in the composite binding pocket which was constructed from combined coordinates of nine NNI compounds from crystal structures of RT complexes. The composite binding pocket of the NNI active site of HIV-1 RT is illustrated as grid lines representing the collective van der Waals surface of nine different inhibitor crystal structures superimposed in the active site and highlight the available space for binding (inhibitor structures include HEPT, MKC, TNK, APA, Nevirapine, *N*-ethyl Nevirapine derivative, 8-Cl TIBO, and two 9-Cl TIBO compounds, with PDB access codes rti, rt1, rt2, hni, vrt, rth, hnv, rev and tvr, respectively). The surface is color-coded for hydrogen bonding (red), hydrophobic (gray) and hydrophilic (blue) groups of the superimposed inhibitors. The hydrogen atoms were not included (see Experimental).





Potential modification sites for PETT derivatives

complex (in this case the RT/9-Cl-TIBO complex). Troviridine derivatives could be viewed as two chemical groups linked together by a thiourea group (Table 1). One half of the molecule is composed of a pyridylthiourea group (compounds **1–9**) which forms an intramolecular hydrogen-bonded heterocyclic ring (shown in troviridine structure). The other half of the molecule is a pyridyl ring separated from the thiocarbonyl group by an ethyl linker. When troviridine was docked into the NNI binding site of RT, it fit into the butterfly-shaped binding region (described by Ding et al.)<sup>19</sup> with one part of the molecule residing in Wing 1 and the other in Wing 2.<sup>23</sup> The ring closest to the thiocarbonyl group resided near the Lys(K)101 loop and the other pyridyl ring was near Trp(W)229. Compounds **1–9** were positioned according to this binding mode into the

**Table 1.** Interaction scores, calculated  $K_i$  values, and measured  $IC_{50}$  data for a series of PETT derivatives

**1–9**

Compd	X	Ms <sup>a</sup> (Å <sup>2</sup> )	Bs <sup>b</sup> (%)	LIPO score	$K_i$ (calcd) (μM) <sup>c</sup>	$IC_{50}$ rRT <sup>*</sup> (μM)	$IC_{50}$ p24 (μM)	SI <sup>d</sup>
<b>1</b>	<i>o</i> -OMe	282	82%	678	1.2	1.0	0.01	$> 1 \times 10^4$
<b>2</b>	<i>o</i> -F	281	82%	674	0.8	0.6	$< 0.001$	$> 1 \times 10^5$
<b>3</b>	<i>o</i> -Cl	285	83%	694	0.5	0.7	$< 0.001$	$> 1 \times 10^5$
<b>4</b>	<i>m</i> -OMe	296	84%	729	0.4	0.4	0.003	$> 3 \times 10^4$
<b>5</b>	<i>m</i> -F	282	83%	687	0.6	0.7	$< 0.001$	$> 1 \times 10^5$
<b>6</b>	<i>m</i> -Cl	283	81%	672	0.8	3.1	N.D.	N.D.
<b>7</b>	<i>p</i> -OMe	302	83%	734	0.6	0.9	0.015	$> 6 \times 10^3$
<b>8</b>	<i>p</i> -F	284	81%	674	7.8	6.4	N.D.	N.D.
<b>9</b>	<i>p</i> -Cl	293	81%	696	4.7	2.5	N.D.	N.D.
Troviridine	N.A.	276	84%	679	0.7	0.8	0.007	$> 1 \times 10^4$
AZT	N.A.	N.A.	N.A.	N.A.	N.A.	$> 100$	0.004	$7 \times 10^3$

<sup>\*</sup>rRT, recombinant HIV reverse transcriptase.

<sup>a</sup>MS, molecular surface area calculated using Connolly's MS program.<sup>31</sup> Defined as boundary of volume within any probe sphere (meant to represent a water molecule) of given radius sharing no volume with hard sphere atoms which make up the molecule. Values are slightly smaller than those approximated by Ludi program.

<sup>b</sup>BS, buried surface: percentage of molecular surface in contact with protein calculated by Ludi based on docked positions. Based on published crystal structures of RT complexes, our calculation shows that these values could be as low as 77% (in RT–HEPT complex) and can be as high as 90% (in RT–APA complex) but most of them average around 84%.

<sup>c</sup>Ludi  $K_i$  values were calculated based on modified empirical score function in the Ludi program (see Experimental).<sup>27,30</sup> Ideal hydrogen bond distances and angles between compounds and protein are assumed in all cases for Ludi Score and  $K_i$  calculation. In published crystal structures of RT complexes, hydrogen bond geometries are indeed close to ideal; the amide carbonyl of residue A101 on a loop demonstrates substantial flexibility which can accommodate the best geometry for hydrogen bonding. The number of rotatable bonds (2, or  $2 + n$  for  $n$  methoxy groups) is used in the Ludi calculation to reflect loss of binding energy due to freezing of internal degrees of freedom.

<sup>d</sup>SI (selectivity index) =  $IC_{50}[MTA]/IC_{50}[p24]$ .  $IC_{50}[MTA]$  values were  $> 100 \mu M$  for compounds **1–9**, as well as troviridine.  $IC_{50}[MTA]$  for AZT was  $50 \mu M$ .

N.D., not determined, for compounds with  $IC_{50}[rRT]$  greater than  $1.0 \mu M$ .

N.A., not applicable.

RT/9-Cl-TIBO active site by a docking procedure (see Experimental) as shown in Figure 2. One of the NH groups of the thiourea part of these compounds consistently formed a hydrogen bond with the backbone of K101. Once the final, energetically favored docked position of the molecule in the NNI site was determined, the molecule was assigned a score, from which an estimation of the inhibition constant ( $K_i$  value) was determined (Table 1). The calculated  $K_i$  values ranging from 0.4  $\mu$ M to 0.8  $\mu$ M suggested that compounds **2–7** would be active inhibitors of RT.

### Methoxy substitutions

The estimated  $K_i$  values generally predicted the trend of the measured  $IC_{50}$ [rRT] values for the inhibition of recombinant HIV RT. Compound **4** had the lowest  $K_i$  value. The docking results showed that the *meta*-methoxy group of **4** is situated near Pro95 and Trp229 in the binding site (distance between closest carbon atoms of m-OMe (**4**) and Pro95 = 3.5 Å, distance between m-OMe (**4**) and Trp229 = 4.0 Å), providing contact with these protein residues which cannot be achieved by trovirdine (Fig. 1). Based on the  $IC_{50}$  [rRT] values of all methoxy compounds, the *meta*-methoxy substituted compound **4**, which had a  $K_i$  value of 0.4  $\mu$ M, showed greater inhibitory activity against recombinant HIV RT and it was approximately twofold more potent than trovirdine ( $IC_{50}$ [rRT] was 0.4  $\mu$ M for compound **4** versus 0.8  $\mu$ M for trovirdine). Compound **4** abrogated HIV replication in human peripheral blood mononuclear cells at nanomolar concentrations with an  $IC_{50}$  value of 3 nM and a selectivity index (SI) of  $>3 \times 10^4$  (Table 1).

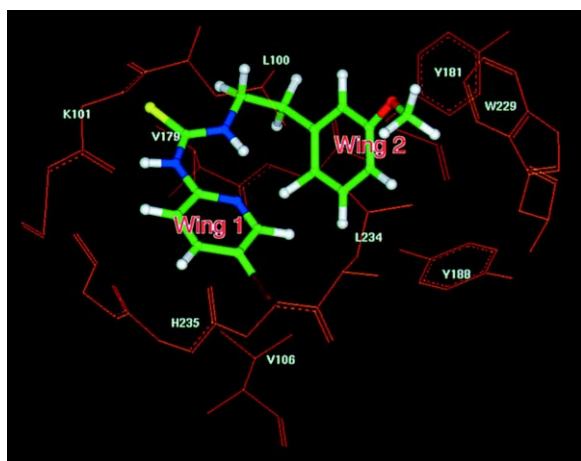


**Figure 2.** The model of compound **4** (color coded by atom type) in NNI binding site of HIV reverse transcriptase, positioned by docking procedure. Wing 1 and Wing 2 represent two different regions of the NNI binding site.

### Fluorine substitutions

Among the fluorine (F) substituted compounds **2**, **5**, and **8**, both *meta* and *ortho* fluoro compounds were at least sevenfold more active than trovirdine ( $IC_{50}$ [p24]  $<1$  nM) (Table 1). Based on the  $IC_{50}$ [rRT] values, compounds with F substitutions at the *meta* and *ortho* positions had nearly the same inhibitory activity against recombinant HIV RT but the para-F substituted compound was 10-fold less active. The color-coded composite binding pocket (Fig. 1) also shows that Wing 2 is mostly hydrophobic except for the region near the *ortho* positions on both sides of the phenyl ring where polar groups such as halogen atoms would be compatible. Trovirdine, however, lacks such ring substituents which could provide favorable interactions with these regions of the binding site. Substitutions at the *meta* position could be on the polar region or the hydrophobic region depending on the chemical group and its consequent conformational change (Fig. 1). The *m*-F substituent of compound **5** (Fig. 3(A)) is probably exposed to the polar (blue) region and therefore is as active as the *o*-F group which would also be exposed to the polar region according to our modeling. The trend in  $IC_{50}$ [rRT] values observed for F-substituted compounds may reflect such a preference. The *p*-F atom, which is small in size but electronegative (more so than chlorine), may not be compatible with the location of the ring plane of nearby hydrophobic Trp229 and could contribute to the lower activity (distance between p-F atom (**8**) and the nearest carbon atom of Trp229 = 4.5 Å). We postulate that this same incompatibility should be observed for any other highly hydrophilic group at the *para* position, and an additional binding penalty should be imposed to better quantitate such features when undertaking modeling studies.

### Chlorine substitutions

Chlorine (Cl) substituted compounds **3**, **6**, and **9** show a trend of observed biological activities which differs from that of both the fluorine and methoxy compounds. Like the *p*-F substituted compound which was less active than other F-substituted compounds, the *p*-Cl compound was less active than the *o*-Cl compound based on the  $IC_{50}$ [rRT] values. Unlike the *m*-F substituted compound which was as active as the *o*-F substituted compound, the *m*-Cl compound was not as active as the *o*-Cl substituted compound. According to our modeling, *o*-Cl is the most likely substituent to be situated near a limited polar (blue) region at Wing 2 (Fig. 3(B)), an interaction which would be favorable. The *o*-Cl compound, like the *o*-F compound discussed above, was more active than trovirdine.

### Hydrophobic group preferred at the *para* position

When  $IC_{50}[rRT]$  values of all compounds with *para* substitutions are compared (7–9), a distinct trend is evident: the *p*-methoxy (OMe) compound (7) is favored over the *p*-halo compounds (8 and 9) (Table 1). Only the *p*-OMe substituted PETT derivative, compound 7, is comparable to trovirdine in its inhibitory activity against recombinant HIV RT. Compound 7 inhibited HIV replication in peripheral blood mononuclear cells with an  $IC_{50}$  value of 15 nM (Table 1). This *p*-OMe preference is consistent with the understanding of the color-coded composite binding pocket at Wing 2, where the binding pocket residues near the *para* position are relatively hydrophobic. We hypothesize that *para* substituted hydrophobic groups positioned near a hydrophobic region of the pocket are most preferred, followed by halogens, and finally hydrophilic groups.

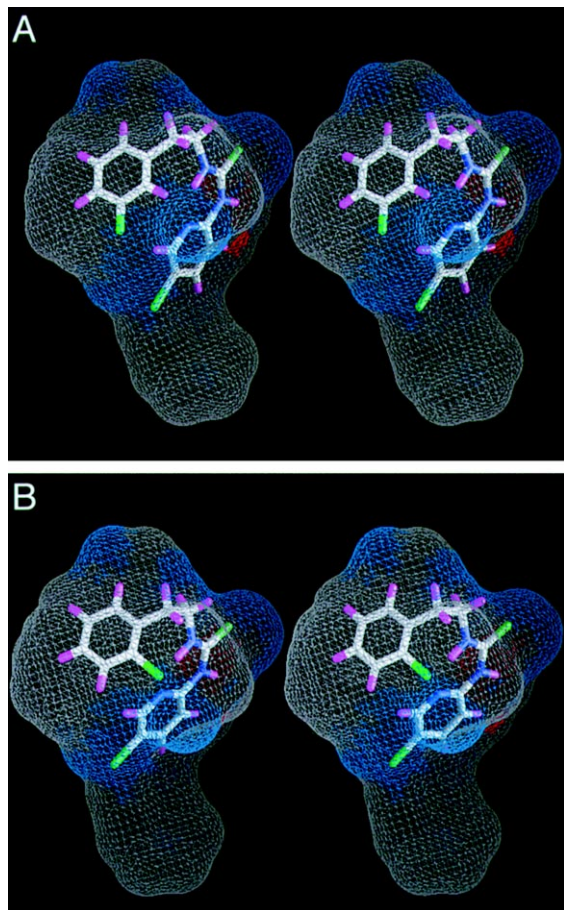


**Figure 3.** Stereoviews of (A) compound 5 (fluorine on phenyl ring is green) (B) and compound 3 (chlorine on phenyl ring is green) in the composite NNI binding pocket of RT which was constructed from combined coordinates of RT complexed with nine different NNI compounds (see Figure 1 and Experimental).

### Conclusions

In summary, our findings revealed the following structure–activity relationships affecting the potency of PETT derivatives with substitutions on various positions of the phenyl ring: (1) methoxy substitution is more favorable at the *meta* position than at the *ortho* or *para* positions; (2) fluorine substitution is favorable at *ortho* and *meta* positions but not at the *para* position; (3) chlorine substitution is favorable only at the *ortho* position; and (4) a hydrophobic group is more desirable than a polar group or hydrophilic group at the *para* position. The use of the composite NNI binding pocket allowed the identification and structure-based design of three promising PETT derivatives with *ortho*-F (2), *ortho*-Cl (3), and *meta*-F (5) substituents on the phenyl ring. These novel PETT derivatives were more active than AZT or trovirdine and showed potent anti-HIV activity with  $IC_{50}[p24]$  values of < 1 nM and selectivity indices (SI) of > 100,000 (Table 1).

### Experimental

#### Construction of the NNI binding pocket

Modeling studies required the construction of a binding pocket which encompassed all RT–NNI complexes with known crystal structures. First, a total of eight coordinates of RT complexes with the compounds HEPT, MKC, TNK, APA, Nevirapine, *N*-ethyl Nevirapine derivative, 9-Cl TIBO (Stuart et al.),<sup>20</sup> and 9-Cl TIBO (Arnold et al.)<sup>24</sup> with PDB access codes 1rti, 1rt1, 1rt2, 1hni, 1vrt, 1rth, 1rev and 1tvr, respectively, were superimposed onto the full coordinates of RT complexed with 8-Cl-TIBO (PDB access code hnv). The ‘thumb’ region of RT complexes are relatively variable compared with the ‘palm’ region. Therefore, a total of 117 C $\alpha$  atoms of the residues from 97 to 213 which cover part of the NNI binding site and the ‘palm’ region were used for a least-squares superimposing procedure within the program O.<sup>25</sup> The RMS values are shown to be 1.00, 0.98, 0.99, 0.62, 0.80, 0.87, 0.94, and 0.65 Å for HEPT, MKC, TNK, APA, Nevirapine, *N*-ethyl Nevirapine derivative and two 9-Cl TIBO complexes, respectively. The coordinates of the corresponding inhibitor molecules were then transformed according to the same matrices derived from the superimposition. Lastly, an overall molecular surface providing a binding pocket encompassing all inhibitors was generated from the overlaid non-hydrogen atom coordinates of all inhibitors using the program GRASP.<sup>26</sup> The surface of the binding pocket was color-coded to reflect characteristics of the overlaid inhibitors, such as hydrogen bonding, hydrophilic, and hydrophobic regions. The nitrogens on the uracil ring of HEPT and TIBO derivatives were



color-coded red for hydrogen-bonding atoms. Oxygen or sulfur atoms of carbonyl, thiocarbonyl, and ester groups, nitrogen atoms of amine groups, and halogen atoms were color-coded blue for polar (hydrophilic) groups. Carbon atoms were considered to be hydrophobic and were colored gray. This pocket, referred to as the composite binding pocket, was used as a basis for the analysis of inhibitor binding to the NNI binding site of HIV RT.

### Docking and $K_i$ prediction

Fixed docking in the Affinity program within InsightII<sup>27</sup> was used for docking small molecules to the NNI binding site which was taken from a crystal structure (PDB code rev, RT/9-Cl-TIBO complex).<sup>24</sup> The program has the ability to define a radius of residues within a 5 Å distance from the NNI molecule. As the modeling calculations progressed, the residues within the defined radius were allowed to move in accordance with energy minimization. Ten final docked positions were initially chosen for each inhibitor modeling calculation but failed to reveal more than two promising positions. Later, only two calculated positions were set for the search target. Calculations were carried out on a SGI INIDIGO2 using the CVFF force field in the Discover program and a Monte Carlo search strategy in Affinity.<sup>28</sup> No solvation procedures were used. Since the total number of movable atoms exceeded 200, conjugated gradient minimization was used instead of the Newton minimization method. The initial coordinates of the compounds were generated using the Sketcher module within InsightII. Each final docking position was then evaluated by a score function in Ludi. The top scoring model was then compared with the composite binding pocket and the known crystal structure of similar compounds and used for further analyses.

We imposed several modifications during the calculation of inhibitory constants ( $K_i$  values) of the positioned compounds using the Ludi score function.<sup>29,30</sup> First, the molecular surface areas (MS) were directly calculated from the coordinates of the compounds in docked conformations using the MS program.<sup>31</sup> Second, we re-evaluated the number of rotatable bonds (NR) which was assessed inaccurately by INSIGHTII (rigidity imposed by hydrogen bonding was not accounted for in the program). Third, we assumed that the conserved hydrogen bond with RT did not deviate significantly from the ideal geometry. This assumption was supported by the fact that in the known crystal structures of RT complexes, all hydrogen bonds between NNIs and RT are near the ideal geometry. Lastly, for the troviridine compounds, we found it necessary to impose an additional penalty for a charged group or halogen atom when positioned near the ring plane of a protein residue

such as tryptophan 229 because the interaction was not adequately accounted for in the Ludi score. The working modification of the Ludi scoring function for the PETT compounds included subtracting a score of P from the total Ludi score when the ring plane of the Trp229 was within 5 Å distance from a *para* substituent (R):

$$\text{Ludi Score} = \text{MS} \times \text{BS} \times 2.93 + 85 \times (\text{of H-bonds}) - \text{NR} \times 24.2 - 100 - \text{P};$$

where

P = 200, when R = a hydrophilic group (e.g. OH or NO<sub>2</sub>);

P = 100, when R = a *para*-halo atom (e.g. F, Cl or Br);

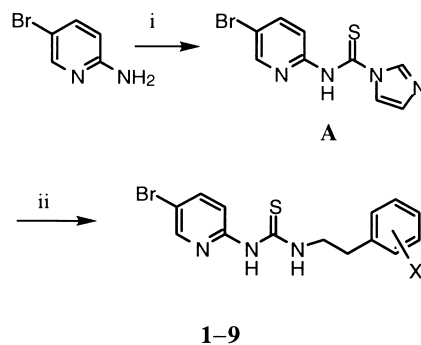
P = 50, when R = a *para*-methoxy (OMe);

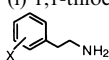
P = 0, when R = a hydrophobic group (e.g. H, CH<sub>3</sub>);

(A more detailed discussion will be published elsewhere.) Consequently, the  $K_i$  values for our modeled compounds were more predictable than they would have been without such modification.<sup>29,30</sup>

### Chemistry

All chemicals were purchased from the Aldrich Chemical Company (Milwaukee, WI). Anhydrous acetonitrile and *N,N*-dimethylformamide were obtained from Aldrich in sure seal bottles and were transferred to reaction vessels via cannula under nitrogen. All reactions were carried out under the atmosphere of nitrogen. Nuclear magnetic resonance (NMR) spectra were recorded on a Varian 300 MHz instrument and chemical shifts ( $\delta$ ) are reported in parts per million (ppm) relative to tetramethyl silane as an internal standard. Splitting patterns are designated as follows: s = singlet, d = doublet, t = triplet, q = quartet, m = multiplet, br = broad peak. <sup>13</sup>C NMR spectra were recorded in CDCl<sub>3</sub> on the same instrument using the proton decoupling technique. The chemical shifts reported for <sup>13</sup>C NMR are referenced to chloroform at 77.0 ppm. <sup>19</sup>F NMR spectra were



**Scheme 1.** Reagents and conditions: (i) 1,1-thiocarbonyldiimidazole, acetonitrile, rt, 12 h; (ii) DMF, , 100 °C, 15 h.

recorded in  $\text{CDCl}_3$  and a 1% solution of trifluoroacetic acid in water was used as an internal standard in a fused capillary tube. Melting points were obtained using a Fisher-Johns melting apparatus and are uncorrected. UV spectra were recorded from a Beckmann Model # DU 7400 UV/Vis spectrometer using a cell path length of 1 cm. Fourier transform infrared spectra were recorded using an FT-Nicolet model Protege #460 instrument. Mass spectra analysis were conducted using a Hewlett-Packard Matrix Assisted Laser Desorption Time-of-Flight (MALDI-TOF) spectrometer model # G2025A. The matrix used was cyanohydroxycinnamic acid. Column chromatography was performed using EM Science silica gel 60. The solvents used for elution varied depending on the compound and included one of the following: ethyl acetate, methanol, chloroform, hexane, methylene chloride or ether. Elemental analysis was performed by Atlantic Microlabs (Norcross, GA).

### General procedure for synthesis

As shown in Scheme 1, compounds **1–9** were synthesized by following the methods used for the synthesis of PETT derivatives.<sup>11</sup> In brief, 2-amino-5-bromopyridine was condensed with 1,1-thiocarbonyl diimidazole to furnish the precursor thiocarbonyl derivative (**A**). Further reaction with appropriately substituted phenylethyl amine gave the target PETT derivatives in good yields.

Specifically, thiocarbonyldiimidazole (8.90 g, 50 mmol) and 2-amino-5-bromo pyridine (8.92 g, 50 mmol) were added to 50 mL of dry acetonitrile at room temperature. The reaction mixture was stirred for 12 h and the precipitate filtered, washed with cold acetonitrile (2×25 mL), and dried under vacuum to afford (11.40 g, 80%) of compound **A**. To a suspension of compound **A** (0.55 mmol) in *N,N*-dimethylformamide (15 mL) an appropriate amine (0.50 mmol) was added. The reaction mixture was heated to 100 °C and stirred for 15 h. The reaction mixture was poured into ice-cold water and the suspension was stirred for 30 min. The product was filtered, washed with water, dried, and further purified by column chromatography to furnish the target compounds **1–9** in good yields.

### Physical data of synthesized compounds 1–9

***N*-[2-(2-Methoxyphenethyl)]-*N'*-[2-(5-bromopyridyl)]-thio-urea (**1**).** Yield: 65%; mp 143–145 °C; UV (MeOH)  $\lambda_{\text{max}}$ : 202, 205, 275 and 306 nm; IR (KBr)  $\nu$  3211, 3153, 3036, 2956, 2835, 1593, 1533, 1462, 1242, 1186, 1036, 1007, 862, 812, 756, 708  $\text{cm}^{-1}$ ;  $^1\text{H}$  NMR ( $\text{CDCl}_3$ )  $\delta$  11.22 (br s, 1H), 9.37 (br s, 1H), 8.02–8.01 (d, 1H), 7.69–7.65 (dd, 1H), 7.28–7.18 (m, 2H), 6.94–6.80 (m, 3H), 4.04–3.98 (q, 2H), 3.81 (s, 3H), 3.04–2.99 (t, 2H);  $^{13}\text{C}$  NMR( $\text{CDCl}_3$ )  $\delta$  178.7, 157.6, 151.7, 146.3, 141.0, 130.7,

127.9, 126.8, 120.3, 113.5, 112.5, 110.3, 55.2, 45.6, 29.8; Maldi ToF found: 366.0 ( $M+1$ ), calcd.: 365.0; Anal. ( $\text{C}_{15}\text{H}_{16}\text{BrN}_3\text{OS}$ ) C, H, N, S.

***N*-[2-(2-Fluorophenethyl)]-*N'*-[2-(5-bromopyridyl)]-thio-urea (**2**).** Yield: 71%; mp 156–157 °C; UV (MeOH)  $\lambda_{\text{max}}$ : 209, 256, 274 and 305 nm; IR (KBr)  $\nu$  3446, 3234, 3163, 3055, 2935, 1672, 1595, 1560, 1531, 1466, 1390, 1362, 1311, 1265, 1227, 1169, 1136, 1089, 1003, 864, 825, 756  $\text{cm}^{-1}$ ;  $^1\text{H}$  NMR ( $\text{CDCl}_3$ )  $\delta$  11.36 (br s, 1H), 9.47 (br s, 1H), 8.05–8.04 (d, 1H), 7.72–7.68 (dd, 1H), 7.30–7.03 (m, 4H), 6.87–6.84 (d, 1H), 4.06–3.99 (q, 2H), 3.10–3.05 (t, 2H);  $^{13}\text{C}$  NMR ( $\text{CDCl}_3$ )  $\delta$  179.1, 163.1, 159.8, 151.7, 146.2, 141.1, 131.2, 131.1, 128.5, 128.4, 124.1, 115.5, 115.2, 113.6, 112.2, 45.8 and 28.2;  $^{19}\text{F}$  NMR ( $\text{CDCl}_3$ )  $\delta$  –42.58 and –42.55 (d); Maldi ToF found: 355.0 ( $M+1$ ), calcd: 354.0; Anal. ( $\text{C}_{14}\text{H}_{13}\text{BrFN}_3\text{S}$ ) C, H, N, S.

***N*-[2-(2-Chlorophenethyl)]-*N'*-[2-(5-bromopyridyl)]-thio-urea (**3**).** Yield: 72%; mp 137–139 °C; UV (MeOH)  $\lambda_{\text{max}}$ : 208, 213, 256, 275 and 305 nm; IR (KBr)  $\nu$  3433, 3221, 3157, 3089, 3037, 2922, 2866, 1668, 1597, 1535, 1466, 1338, 1263, 1209, 1188, 1130, 1095, 1053, 1001, 864, 823, 750  $\text{cm}^{-1}$ ;  $^1\text{H}$  NMR ( $\text{CDCl}_3$ )  $\delta$  11.41 (br s, 1H), 9.54 (br s, 1H), 8.17–8.16 (d, 1H), 7.83–7.79 (dd, 1H), 7.50–7.30 (m, 4H), 6.97–6.94 (d, 1H), 4.19–4.13 (q, 2H), 3.30–3.26 (t, 2H);  $^{13}\text{C}$  NMR ( $\text{CDCl}_3$ )  $\delta$  179.2, 151.7, 146.3, 141.2, 136.3, 134.2, 131.1, 129.6, 128.1, 126.8, 113.6, 112.7, 45.2, and 32.5; Maldi ToF found: 371.8 ( $M+1$ ), calcd: 371.0; Anal. ( $\text{C}_{14}\text{H}_{13}\text{BrClN}_3\text{S}$ ) C, H, N, S, Br.

***N*-[2-(3-Methoxyphenethyl)]-*N'*-[2-(5-bromopyridyl)]-thio-urea (**4**).** Yield: 68%; mp 155–156 °C; UV (MeOH)  $\lambda_{\text{max}}$ : 208, 274 and 306 nm; IR (KBr)  $\nu$  3454, 3236, 3147, 3030, 2951, 2869, 2827, 1591, 1545, 1525, 1466, 1304, 1265, 1229, 1188, 1151, 1095, 1051, 1024, 980, 860, 825, 789, 698  $\text{cm}^{-1}$ ;  $^1\text{H}$  NMR ( $\text{CDCl}_3$ )  $\delta$  11.30 (br s, 1H), 9.25 (br s, 1H), 8.05–8.04 (d, 1H), 7.71–7.67 (dd, 1H), 7.29–7.24 (t, 1H), 6.89–6.78 (m, 4H), 4.05–3.99 (q, 2H), 3.81 (s, 3H), 3.00–2.96 (t, 2H);  $^{13}\text{C}$  NMR ( $\text{CDCl}_3$ )  $\delta$  178.9, 159.7, 151.6, 146.4, 141.1, 140.3, 129.6, 121.2, 115.0, 113.4, 112.7, 111.6, 55.1, 47.1 and 34.8; Maldi ToF found: 367.0 ( $M+2$ ), calcd: 365.0; Anal. ( $\text{C}_{15}\text{H}_{16}\text{BrN}_3\text{OS}$ ) C, H, N, S.

***N*-[2-(3-Fluorophenethyl)]-*N'*-[2-(5-bromopyridyl)]-thio-urea (**5**).** Yield: 73%; mp 171–172 °C; UV (MeOH)  $\lambda_{\text{max}}$ : 202, 208, 258, 275 and 306 nm; IR (KBr)  $\nu$  3213, 3155, 3084, 3028, 2866, 1595, 1533, 1477, 1336, 1308, 1229, 1211, 1173, 1136, 1092, 1026, 935, 870, 827, 791, 740  $\text{cm}^{-1}$ ;  $^1\text{H}$  NMR ( $\text{CDCl}_3$ )  $\delta$  11.33 (br s, 1H), 9.46 (br s, 1H), 8.05–8.04 (d, 1H), 7.73–7.69 (dd, 1H), 7.31–7.26 (m, 1H), 7.08–6.97 (m, 3H), 6.87–6.83 (d, 1H), 4.06–3.99 (q, 2H), 3.05–3.00 (t, 2H);  $^{13}\text{C}$  NMR ( $\text{CDCl}_3$ )  $\delta$  179.1, 163.1, 159.6, 151.7, 146.2, 141.2, 130.1, 129.9, 124.5, 115.9, 115.6, 113.7, 113.5, 113.4, 112.8, 46.7 and 34.6;  $^{19}\text{F}$

NMR (CDCl<sub>3</sub>)  $\delta$  –37.30 and –37.33 (d); Maldi ToF found: 354.0 (M<sup>+</sup>), calcd: 354.0; Anal. (C<sub>14</sub>H<sub>13</sub>BrFN<sub>3</sub>S) C, H, N, S.

***N*-[2-(3-Chlorophenethyl)]-*N'*-[2-(5-bromopyridyl)]-thiourea (6).** Yield: 72%; mp 163–165 °C; UV (MeOH)  $\lambda_{\text{max}}$ : 202, 213, 258, 276 and 305 nm; IR (KBr)  $\nu$  3242, 3161, 3043, 2929, 1593, 1579, 1547, 1527, 1466, 1313, 1227, 1167, 1095, 997, 889, 827, 812, 785, 700 cm<sup>–1</sup>; <sup>1</sup>H NMR (CDCl<sub>3</sub>)  $\delta$  11.33 (br s, 1H), 9.37 (br s, 1H), 8.09–8.08 (d, 1H), 7.73–7.69 (dd, 1H), 7.28–7.15 (m, 4H), 6.85–6.82 (d, 1H), 4.04–3.98 (q, 2H), 3.02–2.97 (t, 2H); <sup>13</sup>C NMR (CDCl<sub>3</sub>)  $\delta$  179.1, 151.6, 146.3, 141.2, 140.7, 134.2, 129.8, 129.0, 127.0, 126.8, 113.4, 112.8, 46.7 and 34.5; Maldi ToF found: 371.8 (M + 1), calcd: 371.0; Anal. (C<sub>14</sub>H<sub>13</sub>BrClN<sub>3</sub>S) C, H, N, S.

***N*-[2-(4-Methoxyphenethyl)]-*N'*-[2-(5-bromopyridyl)]-thiourea (7).** Yield: 85%; mp 178–179 °C; UV (MeOH)  $\lambda_{\text{max}}$ : 205, 226, 275 and 305 nm; IR (KBr)  $\nu$  3221, 3159, 3042, 2931, 2827, 1587, 1510, 1464, 1311, 1225, 1165, 1088, 1034, 820, 773, 708 cm<sup>–1</sup>; <sup>1</sup>H NMR (CDCl<sub>3</sub>)  $\delta$  11.30 (br s, 1H), 9.87 (br s, 1H), 8.00–7.99 (d, 1H), 7.67–7.63 (dd, 1H), 7.21–7.18 (d, 2H), 6.95–6.85 (m, 3H), 4.00–3.93 (q, 2H), 3.81 (s, 3H), 2.96–2.92 (t, 2H); <sup>13</sup>C NMR (CDCl<sub>3</sub>)  $\delta$  179.1, 158.0, 151.9, 145.8, 140.7, 130.6, 129.6, 113.8, 113.7, 112.1, 55.1, 46.9 and 33.8; Maldi ToF found: 366.0 (M + 1), calcd: 365.0; Anal. (C<sub>15</sub>H<sub>16</sub>BrN<sub>3</sub>OS) C, H, N, S.

***N*-[2-(4-Fluorophenethyl)]-*N'*-[2-(5-bromopyridyl)]-thiourea (8).** Yield: 69%; mp 177–178 °C; UV (MeOH)  $\lambda_{\text{max}}$ : 208, 211, 274 and 306 nm; IR (KBr)  $\nu$  3456, 3213, 3155, 3086, 3028, 2868, 1595, 1560, 1533, 1477, 1336, 1308, 1238, 1211, 1173, 1136, 1092, 1026, 933, 869, 827, 791, 741, 694 cm<sup>–1</sup>; <sup>1</sup>H NMR (CDCl<sub>3</sub>)  $\delta$  11.29 (br s, 1H), 9.27 (br s, 1H), 8.04–8.03 (d, 1H), 7.73–7.69 (dd, 1H), 7.27–7.22 (m, 2H), 7.04–6.99 (m, 2H), 6.83–6.79 (d, 1H), 4.03–3.96 (q, 2H), 3.02–2.97 (t, 2H); <sup>13</sup>C NMR (CDCl<sub>3</sub>)  $\delta$  179.1, 163.2, 159.2, 151.6, 146.3, 141.2, 134.3, 130.3, 130.2, 115.4, 115.2, 113.5, 112.8, 47.0, and 34.1; <sup>19</sup>F NMR (CDCl<sub>3</sub>)  $\delta$  –40.55 (m); Maldi ToF found: 354.8 (M + 1), calcd: 354.0; Anal. (C<sub>14</sub>H<sub>13</sub>BrFN<sub>3</sub>S) C, H, N, S.

***N*-[2-(4-Chlorophenethyl)]-*N'*-[2-(5-bromopyridyl)]-thiourea (9).** Yield: 71%; mp 180–183 °C; UV (MeOH)  $\lambda_{\text{max}}$ : 206, 209, 219, 256, 275 and 305 nm; IR (KBr)  $\nu$  3221, 3153, 3086, 3022, 2931, 1674, 1593, 1562, 1533, 1473, 1406, 1340, 1304, 1265, 1227, 1169, 1138, 1092, 1016, 820, 752, 714 cm<sup>–1</sup>; <sup>1</sup>H NMR (CDCl<sub>3</sub>)  $\delta$  11.40 (br s, 1H), 9.34 (br s, 1H), 8.15–8.14 (d, 1H), 7.84–7.80 (dd, 1H), 7.46–7.30 (m, 4H), 6.92–6.89 (d, 1H), 4.10–4.07 (q, 2H), 3.13–3.08 (t, 2H); <sup>13</sup>C NMR (CDCl<sub>3</sub>)  $\delta$  179.2, 151.6, 146.3, 141.3, 137.1, 130.2, 128.6, 113.5, 112.8, 46.8 and 34.2; Maldi ToF found: 372.0 (M + 1), calcd: 371.0; Anal. (C<sub>14</sub>H<sub>13</sub>BrClN<sub>3</sub>S) C, H, N, S.

**Stock HTLVIII virus.** The HIV-1 strain HTLVIII (kindly provided by Dr. Neal T. Wetherall, VIROMED Laboratories, Inc.), which was propagated in CCRF-CEM cells, was used in in vitro assays of the anti-HIV-1 activity of the synthesized novel PETT derivatives. Cell-free supernatants of HTLVIII-infected CCRF-CEM cells were harvested, dispensed into 1 mL aliquots, and frozen at –70 °C. Periodic titration of stock virus was performed by examining its cytopathic effects in MT-2 cells.<sup>32</sup>

**In vitro assays of anti-HIV-1 activity.** Normal human peripheral blood mononuclear cells (PBMNC) from HIV-negative donors were cultured 72 h in RPMI 1640 supplemented with 20%(v/v) heat-inactivated fetal bovine serum (FBS), 3% interleukin-2, 2 mM L-glutamine, 25 mM HEPES, 2 g/L NaHCO<sub>3</sub>, 50 µg/mL gentamicin, and 4 µg/mL phytohemagglutinin prior to exposure to HIV-1 at a multiplicity of infection (MOI) of 0.1 during a 1 h adsorption period at 37 °C in a humidified 5% CO<sub>2</sub> atmosphere. Subsequently, cells were cultured in 96-well microtiter plates (100 µL/well; 2 × 10<sup>6</sup> cells/mL) in the presence of various concentrations of PETT analogues or AZT and aliquots of culture supernatants were removed from the wells on the 7th day after infection for p24 antigen assays, as previously described.<sup>32–34</sup> The applied p24 enzyme immunoassay (EIA) was the unmodified kinetic assay commercially available from Coulter Corporation/Immunotech, Inc. (Westbrooke, ME), which utilizes a murine mAb to HIV core protein coated onto microwell strips to which the antigen present in the test culture supernatant samples binds. Percent viral inhibition was calculated by comparing the p24 values from the test substance-treated infected cells with p24 values from untreated infected cells (i.e. virus controls). In addition, the IC<sub>50</sub> values measuring the activity of compounds against recombinant HIV-1 RT (rRT) were determined using the Quant-RT assay system (Amersham, Arlington Heights, IL, USA), which utilizes the scintillation proximity assay principle.<sup>35</sup> In parallel, the effects of various treatments on cell viability were also examined, as described.<sup>32,33</sup> In brief, non-infected PBMNC were treated with PETT analogues for 7 days under identical experimental conditions. A Microculture Tetrazolium Assay (MTA), using 2,3-bis(2-methoxy-4-nitro-5-sulfophenyl)-5-[(phenylamino)-carbonyl]-2H-tetrazolium hydroxide (XTT), was performed to quantitate cellular proliferation.

## References

- Greene, W. C. *New Engl. J. Med.* **1991**, 324, 308.
- Mitsuya, H.; Yarchoan, R.; Broder, S. *Science* **1990**, 249, 1533.
- De Clercq, E. J. *Acqu. Imm. Defic. Syndr. Res. Hum. Retrovirus* **1992**, 8, 119.
- Pauwels, R.; Andries, K.; Desmyter, J.; Schols, D.; Kukla, M. J.; Breslin, H. J.; Raeymaeckers, A.; Van Gelder, J.; Woes-



- tenborghs, R.; Heykants, J.; Schellekens, K.; Janssen, M. A. C.; De Clercq, E.; Janssen, P. A. *Nature* **1990**, *343*, 470.
5. Tanaka, H.; Baba, M.; Hayakawa, H.; Sakamaki, T.; Miyasaka, T.; Ubasawa, M.; Takashima, H.; Sekiya, K.; Nitta, I.; Shigeta, S.; Walker, R. T.; Balzarini, J.; De Clercq, E. *J. Med. Chem.* **1991**, *34*, 349.
6. Pontikis, R.; Benhida, R.; Aubertin, A. M.; Grierson, D. S.; Monneret, C. *J. Med. Chem.* **1997**, *40*, 1845.
7. Danel, K.; Larsen, E.; Pedersen, E. B.; Vestergaard, B. F.; Nielsen, C. *J. Med. Chem.* **1996**, *39*, 2427.
8. Baba, M.; Shigeta, S.; Tanaka, H.; Miyasaka, T.; Ubasawa, M.; Umez, K.; Walker, R. T.; Pauwels, R.; De Clercq, E. *Antiviral Res.* **1992**, *17*, 245.
9. Romero, D. L.; Morge, R. A.; Genin, M. J.; Biles, C.; Busso, M.; Resnick, L.; Althaus, I. W.; Reusser, F.; Thomas, R. C.; Tarpley, W. G. *J. Med. Chem.* **1993**, *36*, 1505.
10. Balzarini, J.; Perez Perez, M. J.; San Felix, A.; Schols, D.; Perno, C. F.; Vandamme, A. M.; Camarasa, M. J.; De Clercq, E. *Proc. Natl. Acad. Sci. U.S.A.* **1992**, *89*, 4392.
11. Bell, F. W.; Cantrell, A. S.; Hogberg, M.; Jaskunas, S. R.; Johansson, N. G.; Jordan, C. L.; Kinnick, M. D.; Lind, P.; Morin, J. M., Jr.; Noreen, R.; Oberg, B.; Palkowitz, J. A.; Parrish, C. A.; Pranc, P.; Sahlberg, C.; Ternansky, R. T.; Vasileff, R. T.; Vrang, L.; West, S. J.; Zhang, H.; Zhou, X. X. *J. Med. Chem.* **1995**, *38*, 4929.
12. Cantrell, A. S.; Engelhardt, P.; Hogberg, M.; Jaskunas, S. R.; Johansson, N. G.; Jordan, C. L.; Kangasmetsa, J.; Kinnick, M. D.; Lind, P.; Morin, J. M., Jr.; Muesing, M. A.; Noreen, R.; Oberg, B.; Pranc, P.; Sahlberg, C.; Ternansky, R. J.; Vasileff, R. T.; Vrang, L.; West, S. J.; Zhang, H. *J. Med. Chem.* **1996**, *39*, 4261.
13. Ahgren, C.; Backro, K.; Bell, F. W.; Cantrell, A. S.; Clemens, M.; Colacino, J. M.; Deeter, J. B.; Engelhardt, J. A. M. H.; Jaskunas, S. R.; Johansson, N. G.; Jordan, C. L.; Kasher, J. S.; Kinnick, M. D.; Lind, P.; Lopez, C.; Morin, J. M. J.; Muesing, M. A.; Noreen, R.; Oberg, B.; Paget, C. J.; Palkowitz, J. A.; Parrish, C. A.; Pranc, P.; Rippey, M. K.; Rydergard, C.; Sahlberg, C.; Swanson, S.; Ternansky, R. J.; Unge, T.; Vasileff, R. T.; Vrang, L.; West, S. J.; Zhang, H.; Zhou, X. X. *Antimicrob. Agents Chemother.* **1995**, *39*, 1329.
14. Heinisch, G.; Matuszczak, B.; Pachler, S.; Rakowitz, D. *Antiviral Chem. Chemother.* **1997**, *8*, 443.
15. Kohlstaedt, L. A.; Wang, J.; Friedman, J. M.; Rice, P. A.; Steitz, T. A. *Science* **1992**, *256*, 1783.
16. Smerdon, S. J.; Jager, J.; Wang, J.; Kohlstaedt, L. A.; Chirino, A. J.; Friedman, J. M.; Rice, P. A.; Steitz, T. A. *Proc. Natl. Acad. Sci. U.S.A.* **1994**, *91*, 3911.
17. Ren, J.; Esnouf, R.; Garman, E.; Somers, D.; Ross, C.; Kirby, I.; Keeling, J.; Darby, G.; Jones, Y.; Stuart, D.; Stammers, D. *Nat. Struct. Biol.* **1995**, *2*, 293.
18. Ding, J.; Das, K.; Tantillo, C.; Zhang, W.; Clark, A. D., Jr.; Jessen, S.; Lu, X.; Hsiou, Y.; Jacobo Molina, A.; Andries, K.; Pauwels, R.; Moereels, H.; Koymans, L.; Janssen, P. A. J.; Smith, R. H. J.; Kroeger Koepke, R.; Michejda, C. J.; Hughes, S. H.; Arnold, E. *Structure* **1995**, *3*, 365.
19. Ding, J.; Das, K.; Moereels, H.; Koymans, L.; Andries, K.; Janssen, P. A.; Hughes, S. H.; Arnold, E. *Nat. Struct. Biol.* **1995**, *2*, 407.
20. Ren, J.; Esnouf, R.; Hopkins, A.; Ross, C.; Jones, Y.; Stammers, D.; Stuart, D. *Structure* **1995**, *3*, 915.
21. Hopkins, A. L.; Ren, J.; Esnouf, R. M.; Willcox, B. E.; Jones, E. Y.; Ross, C.; Miyasaka, T.; Walker, R. T.; Tanaka, H.; Stammers, D. K.; Stuart, D. I. *J. Med. Chem.* **1996**, *39*, 1589.
22. Kroeger Smith, M. B.; Rouzer, C. A.; Taneyhill, L. A.; Smith, N. A.; Hughes, S. H.; Boyer, P. L.; Janssen, P. A.; Moereels, H.; Koymans, L.; Arnold, E.; Ding, J.; Das, K.; Zhang, W.; Michejda, C. J.; Smith, R. H. *Protein Sci.* **1995**, *4*, 2203.
23. Mao, C.; Vig, R.; Sudbeck, E. A.; Venkatachalam, T. K.; Uckun, F. M. Submitted.
24. Das, K.; Ding, J.; Hsiou, Y.; Clark, A. D., Jr.; Moereels, H.; Koymans, L.; Andries, K.; Pauwels, R.; Janssen, P. A.; Boyer, P. L.; Clark, P.; Smith, R. H., Jr.; Kroeger Smith, M. B.; Michejda, C. J.; Hughes, S. H.; Arnold, E. *J. Mol. Biol.* **1996**, *264*, 1085.
25. Jones, T. A.; Zou, J. Y.; Cowan, S. W.; Kjeldgaard, G. *Acta Crystallogr. A* **1991**, *47*, 110.
26. Nicholls, A.; Sharp, K.; Honig, B. GRASP Graphical representation and analysis of surface properties. *Prot. Struct. Funct. Genet.*, **1991**, *11*, 281.
27. InsightII, Molecular Simulations Inc. **1996**, San Diego, CA.
28. Luty, B. A.; Wasserman, P. F.; Stouten, P. F.; Hodge, C. N.; Zacharias, M.; McCammon, J. A. *J. Comp. Chem.* **1995**, *16*, 454.
29. Bohm, H. J. *J. Comput. Aided Mol. Des.* **1992**, *6*, 593.
30. Bohm, H. J. *J. Comput. Aided Mol. Des.* **1994**, *8*, 243.
31. Connolly, M. L. *Science* **1983**, *221*, 709.
32. Erice, A.; Lieler, C. L.; Meyers, D. E.; Sannerund, K. J.; Irvin, J. D.; Balfour, H. H.; Uckun, F. M. *Antimicrob. Agents Chemother.* **1993**, *37*, 835.
33. Zarling, J. M.; Moran, P. A.; Haffar, O.; Sias, J.; Richman, D. D.; Spina, C. A.; Myers, D. E.; Kuebelbeck, V.; Ledbetter, J. A.; Uckun, F. M. *Nature* **1990**, *347*, 92.
34. Uckun, F. M.; Chelstrom, L. M.; Tuel-Ahlgren, L.; Dibirdik, I.; Irvin, J. D.; Chandan-Langlie, M.; Myers, D. E. *Antimicrob. Agents Chemother.* **1998**, *42*, 383.
35. Bosworth, N.; Towers, P. *Nature* **1989**, *341*, 167.